

# Flat band superconductivity in type-II Weyl-semimetal $\text{WTe}_2$ induced by a normal metal contact

Artem Kononov,<sup>1,\*</sup> Martin Endres,<sup>1</sup> Gulibusitan Abulizi,<sup>1</sup> Kejian Qu,<sup>2</sup> Jiaqiang Yan,<sup>3,2</sup> David G. Mandrus,<sup>2,3</sup> Kenji Watanabe,<sup>4</sup> Takashi Taniguchi,<sup>4</sup> and Christian Schenberger<sup>1,5,†</sup>

<sup>1</sup>*Department of Physics, University of Basel, Klingelbergstrasse 82, CH-4056 Basel, Switzerland*

<sup>2</sup>*Department of Materials Science and Engineering, University of Tennessee, Knoxville, TN 37996, United States*

<sup>3</sup>*Materials Science and Technology Division, Oak Ridge National Laboratory, Oak Ridge, TN 37831, United States*

<sup>4</sup>*National Institute for Material Science, 1-1 Namiki, Tsukuba 305-0044, Japan*

<sup>5</sup>*Swiss Nanoscience Institute, University of Basel, Klingelbergstrasse 82, CH-4056 Basel, Switzerland*

$\text{WTe}_2$  is a material with rich topological properties: it is a 2D topological insulator as a monolayer and a Weyl-semimetal and higher-order topological insulator (HOTI) in the bulk form. Inducing superconductivity in topological materials is a way to obtain topological superconductivity, which lays at the foundation for many proposals of fault tolerant quantum computing. Here, we demonstrate the emergence of superconductivity at the interface between  $\text{WTe}_2$  and the normal metal palladium. The superconductivity has a critical temperature of about 1.2 K. By studying the superconductivity in perpendicular magnetic field, we obtain the coherence length and the London penetration depth. These parameters hint to a possible origin of superconductivity due to the formation of flat bands. Furthermore, the critical in-plane magnetic field exceeds the Pauli limit, suggesting a non-trivial nature of the superconducting state.

## INTRODUCTION

Topological materials attract a lot of attention in modern condensed matter physics. This interest stems from intriguing fundamental properties and great potential for practical applications. The especially interesting class of topological materials are topological superconductors, promising to revolutionize quantum computing due to the inherent error protection [1]. Topological superconductivity could be obtained by inducing superconductivity in topologically non-trivial system. There are several theoretical predictions of different topological superconducting states in Dirac and Weyl semimetal based systems, including Fulde-Ferrell-Larkin-Ovchinnikov superconductors [2–4], the time-reversal invariant topological superconductor [5], chiral non-Abelian Majorana fermions [6], and flat band superconductivity [7].

$\text{WTe}_2$  is a layered transition-metal dichalcogenide with rich topological properties. As a bulk material it is a type-II Weyl semimetal with bulk Weyl nodes connected by Fermi arcs surface states [8, 9]. Recently, it has been predicted to be a higher-order topological insulator with one-dimensional hinge states [10], experimental evidence of these states has been obtained [11–13]. In a single layer form,  $\text{WTe}_2$  is a two-dimensional topological insulator with helical edge states [14, 15]. In addition to all these topological phases  $\text{WTe}_2$  has a tendency of becoming superconducting under different conditions: under pressure [16, 17], electron doping [18] or electrostatic gating [19, 20]. Combination of these properties makes  $\text{WTe}_2$  particularly promising candidate for topological superconductivity.

In this manuscript we demonstrate the emergence of superconductivity at the interface between the normal metal palladium and few-layer thick  $\text{WTe}_2$ . Studying

the transport properties in magnetic field and at different temperatures we deduce the main parameters characterizing the superconducting state including the critical temperature, the coherence length and the London penetration depth. These parameters hint to a possible origin of superconductivity due to the formation of flat bands. Moreover, the measured in-plane critical field exceeds the Pauli limit, suggesting non-trivial superconducting pairing. The coexistence of the observed superconductivity with topological states in  $\text{WTe}_2$  makes it a promising platform for studying topological superconductivity and applications for quantum computing.

## EXPERIMENT

The single crystals of  $\text{WTe}_2$  were grown with a flux growth method [21]. We obtained few-layer thick  $\text{WTe}_2$  flakes by mechanically exfoliating single crystals with an adhesive tape on oxidized Si substrate with 295 nm  $\text{SiO}_2$  layer. To avoid oxidation of  $\text{WTe}_2$  the exfoliation has been carried out in a glovebox with low oxygen content. Suitable flakes have been identified with an optical contrast method [22] and were picked up and transferred using the polycarbonate assisted pick-up technique [23] on to the device chip that already contained prepatterned contacts. The contacts were defined before using standard e-beam lift-off lithography and metal deposition of 3 nm titanium and 12 nm palladium. In the final stack  $\text{WTe}_2$  is protected from oxidation by an hBN layer that covers the  $\text{WTe}_2$ . All the measurements were performed in the dilution refrigerator with a base temperature of 60 mK.

## RESULTS AND DISCUSSION

Fig. 1(a) shows an optical image of an encapsulated WTe<sub>2</sub> crystals with a contact pattern that resembles a standard Hall-bar configuration. Note, that the visible Pd contacts are at the bottom, followed by a few layer WTe<sub>2</sub> crystal with a rectangular shape and high-aspect ratio oriented vertically, followed by an hBN layer that has the weakest contrast in the image. The drawn electrical schematics corresponds to the measurement of the longitudinal resistance  $R_{xx}$  given by  $V_{xx}/I$ . Fig. 1(b) displays  $R_{xx}$  as a function of perpendicular magnetic field  $B_{\perp}$ . At 4 K the resistance shows a non-saturating magnetoresistance characteristic for WTe<sub>2</sub> [24]. The small thickness of our WTe<sub>2</sub> crystal results in a relatively small magnetoresistance [25]. At lower temperature additional features develop in  $R_{xx}(B_{\perp})$ : at zero field the resistance goes to zero and in small fields it has an intermediate state between zero and high-temperature values. This behavior is a result of the formation of a superconducting state in WTe<sub>2</sub> above the Pd leads. Furthermore, these superconducting regions could be connected by the Josephson effect, as illustrated in Fig. 1(c), leading to a zero longitudinal resistance. The zero resistance state appears only for smaller distances between the contacts excluding intrinsic superconductivity in our WTe<sub>2</sub> samples.

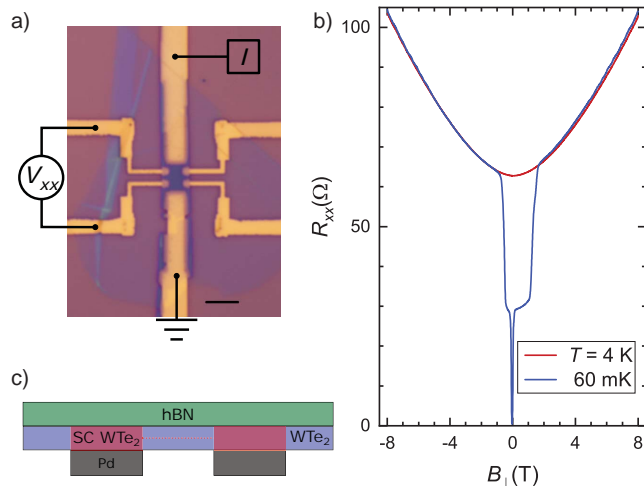


FIG. 1. (a) Optical image of the sample 1 (scale bar 5  $\mu\text{m}$ ) with a sketch of the measurement setup. (b) Longitudinal resistance  $R_{xx} = V_{xx}/I$  as a function of perpendicular magnetic field  $B_{\perp}$ : at 4 K only a non-saturating magnetoresistance is seen, whereas at 60 mK the resistance shows additionally a transition to a smaller value in a magnetic field of  $B_{\perp} \sim 1$  T, and a transition to zero-resistance due to emerging superconductivity for much lower  $B_{\perp}$ . (c) Cross-sectional view through the contact region: The region of WTe<sub>2</sub> above the Pd leads turn into superconducting regions (red). These regions can be connected by the Josephson effect (red dashed line) if not too far apart.

To understand the properties of the superconducting state we studied the evolution of  $R_{xx}(B_{\perp})$  with increasing temperature, as shown in Fig. 2(a). Upon temperature increase both transitions in the resistance are shifting towards zero field. The zero resistance state connected to the Josephson coupling disappears first above 0.75 K, the second transition connected to the suppression of superconductivity by magnetic field  $B_{c2}$  persists up to 1.1 K. We define  $B_{c2}(T)$  as the magnetic field where the  $R_{xx}(B_{\perp})$  crosses the fixed resistance value  $R_{xx} = 45 \Omega$ , which approximately corresponds to half of the resistance step. Fig. 2(b) shows the extracted dependence of the critical magnetic field as a function of temperature  $T$ . The  $B_{c2}(T)$  dependence is linear as expected for a 2D superconductor

$$B_{c2}(T) = \frac{\Phi_0}{2\pi\xi_{GL}^2} \left(1 - \frac{T}{T_c}\right), \quad (1)$$

where  $\Phi_0$  is the magnetic flux quantum,  $\xi_{GL}$  is the Ginzburg-Landau coherence length at zero temperature, and  $T_c$  is the critical temperature at zero magnetic field. Fitting the experimental data with equation 1 we obtain  $T_c \sim 1.2$  K and  $\xi_{GL} \sim 14$  nm. At low temperatures the Ginzburg-Landau coherence length is similar to the BardeenCooperSchrieffer (BCS) coherence length  $\xi_{GL} \sim \xi$ . Knowing the coherence length and the critical temperature, we can estimate the Fermi velocity  $v_F = \xi\pi\Delta/\hbar$ , where we take for  $\Delta(T_c)$  the BCS relation  $\Delta \sim 1.76k_B T_c$ , yielding  $v_F \sim 1.2 \cdot 10^4$  m s<sup>-1</sup>. The obtained Fermi velocity is quite small. This could suggest superconductivity due to the formation of flat bands [26].

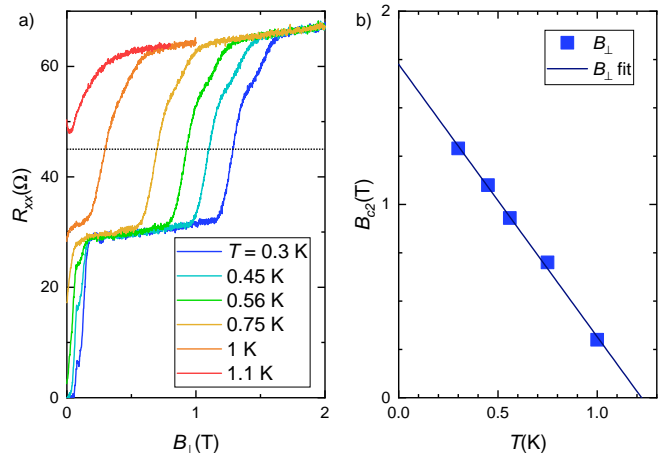


FIG. 2. (a) Longitudinal resistance as a function of perpendicular magnetic field  $B_{\perp}$  at different temperatures. The dotted line indicates the resistance value used to determine  $B_{c2}(T)$ . (b) Critical magnetic field  $B_{c2}$  as function of temperature extracted from (a) and a  $B_{c2} \propto 1/T$  fit of the data.

We further investigate the superconducting properties by looking at the  $R_{xx}$  dependence on the *in-plane* magnetic field  $B_{\parallel}$ , as shown in Fig. 3(a). Compared

with the perpendicular field, both changes in the resistance have shifted to higher magnetic fields. We extracted the critical field values as a function of temperature and plotted them in Fig. 3(b). In this case,  $B_{c2}(T)$  follows the known empirical law for superconductors  $B_{c2}(T) = B_{c2}(0) [1 - (T/T_c)^2]$  [27], as evident from the very good agreement between measured points and the fit. Both fits of the critical field as a function of  $B_{\perp}$  and  $B_{\parallel}$  converge to the same  $T_c \sim 1.2$  K.

A notable feature of the parallel critical field is its large value, which exceeds the Pauli paramagnetic limit  $B_P$ . The later is given by  $B_P \sim 1.76k_B T_c \sqrt{2}/g\mu_B \sim 1.86T_c \sim 2.3$  T. This expression is based on the BCS theory for weak-coupling superconductors and a free electron  $g$ -factor of  $g = 2$  [28]. This effect has also been observed in gated monolayer [19, 20] and doped bulk WTe<sub>2</sub> [18]. Several mechanisms could be responsible for superconductivity exceeding the Pauli limit, including Ising-type superconductivity [28] or a diminishing of the effective  $g$ -factor due to strong spin-orbit coupling [29]. Further studies are required to resolve this puzzle.

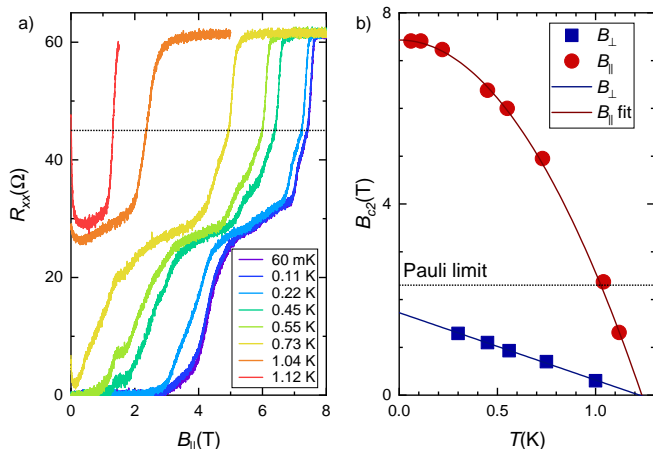


FIG. 3. (a) Longitudinal resistance as a function of in-plane magnetic field at different temperatures. The dotted line indicates resistance level used to determine  $B_{c2}(T)$ . (b) Critical magnetic field as function of temperature extracted from (a) and fit to the data. The dotted line indicated the maximum critical field given by the Pauli limit  $B_P$ , which we estimate to 2.3 T. The data for critical perpendicular magnetic field is shown for comparison.

The London penetration depth  $\lambda_L$  is another important characteristic of a superconductor. While RF-measurements are a common way of measuring the penetration depth [30], it can also be estimated by measuring the critical current of a Josephson junction in magnetic field  $B_{\perp}$ . A Josephson junction placed in a perpendicular magnetic field demonstrates an oscillating critical current. One period of the oscillations corresponds to the magnetic flux quantum  $\Phi_0$  through the effective area of the junction  $S_{eff} = WL_{eff} = W(L + 2\lambda)$ , where  $W$  and  $L$  are the junction's width and length, respectively, and  $\lambda$

is the magnetic field penetration depth [27], see Fig 4(a). For a bulk superconductor  $\lambda = \lambda_L$ , but for a thin film superconductor with thickness  $d$ , the penetration depth is a function of the thickness  $\lambda(d) = \lambda_L \coth(d/\lambda_L)$  [30]. In the limit of small thickness  $d \ll \lambda_L$  the previous expression is equal to the Pearl's penetration depth  $\lambda_P = \lambda_L^2/d$ .

Fig. 4(b) demonstrates several examples of  $I_c(B_{\perp})$  dependencies for Josephson junctions in WTe<sub>2</sub> where the superconducting regions on top of Pd play the role of superconducting contacts. These dependencies have a SQUID-like character due to hinge states [11] with a rapidly decaying Fraunhofer contribution due to the Fermi-arc surface states [31, 32]. The SQUID-like oscillations with many visible periods allow to determine the period with a high precision. For junctions 1 and 2, with  $L = 1$   $\mu\text{m}$  and  $W = 4.3$   $\mu\text{m}$ , we obtain a period of  $\Delta B = 0.27$  mT. This period corresponds to  $L_{eff} = 1.77$   $\mu\text{m}$  and a penetration depth of  $\lambda = 380$  nm. For junction 3 ( $L = 500$  nm,  $W = 4.2$   $\mu\text{m}$ ) we obtain  $\Delta B = 0.41$  mT, yielding  $\lambda = 350$  nm. The obtained penetration depth is much larger than the thickness of the WTe<sub>2</sub> flakes  $d \sim 7$  nm (approximately 10-layers thick) so that the extracted penetration depth is given by Pearl's limit  $\lambda = \lambda_P = \lambda_L^2/d$ . Using this expression we estimate the London penetration depth to be  $\lambda_L \sim 50$  nm. The ratio between the London penetration depth and the coherence length  $\kappa = \lambda_L/\xi$  is  $\kappa \sim 3 > 1/\sqrt{2}$ , suggesting type-II superconductivity [27].

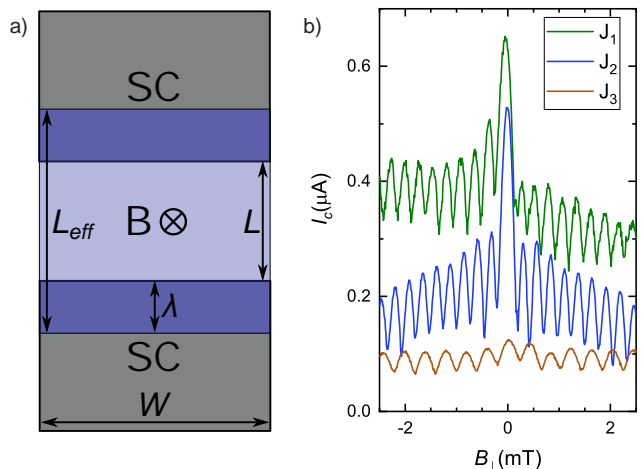


FIG. 4. (a) Illustration of flux focusing in Josephson junction. The area of the junction where the magnetic field is not screened and penetrating the junction is not given by the geometrical area  $W \times L$ , where  $L$  is the junction length, but by an effective area given by  $W \times L_{eff}$ . Here, the effective length  $L_{eff}$  equals  $L + 2\lambda$ , where  $\lambda$  is accounting for the penetration depth of the field into the superconductor. (b) Critical current as a function of magnetic field for three different Josephson junctions. Junctions  $J_1$  and  $J_2$  have  $W = 4.3$   $\mu\text{m}$  and length  $L = 1$   $\mu\text{m}$ , junction  $J_3$  -  $W = 4.2$   $\mu\text{m}$ ,  $L = 500$  nm.

The obtained London penetration depth is comparable

to typical values for metals and is surprisingly small considering the semimetallic nature of WTe<sub>2</sub>. An estimate of the superconducting electron density yields quite high value  $n_s = m/\mu_0\lambda_L^2 e^2 \sim 3 \cdot 10^{21} \text{ cm}^{-3}$ , where  $m \sim 0.3m_e$  is the effective mass of the electrons in WTe<sub>2</sub> [33]. This value is higher than the typical carrier densities in WTe<sub>2</sub>  $n \sim 10^{19} \text{ cm}^{-3}$  [33] and corresponds to a density per single layer of  $n_s^{1L} \sim 2 \cdot 10^{14} \text{ cm}^{-2}$ , which is an order of magnitude higher than the electron density in monolayer WTe<sub>2</sub> with gate induced superconductivity [19, 20], but comparable to the predicted optimal charge carrier density [34]. Furthermore, a large superconducting carrier density implies high density of states at the Fermi level  $g(E_F) \sim n_s/2\Delta \sim 8 \cdot 10^{24} \text{ cm}^{-3} \text{ eV}^{-1}$ , which is a signature of flat bands.

The emergence of superconductivity at the interface of two non-superconducting materials is quite surprising. It has been observed previously in different Weyl and Dirac semimetals [35–37]. However, there is no clear understanding of its origin. We think that in our samples two effects could play a role. First, electron doping from palladium [38] could create a superconducting state similar to what was seen in monolayer [19, 20] or bulk doped WTe<sub>2</sub> [18]. Such a high doping could explain the observed high density of superconducting electrons. On the other hand, this explanation is at odds with the observed small Fermi velocity. In contrast, the formation of flat bands [39] could explain both the high carrier density and the low Fermi velocity. Flat bands are ubiquitous in van der Waals heterostructure. For example, high carrier-density combined with a low Fermi velocity has been observed close to van-Hove singularities in the band structure of superlattices formed in hBN-encapsulated graphene [40]. It can also be formed due to strain at the interface [7, 41]. The presence of the flat bands is known to stimulate superconductivity [26, 42, 43].

## CONCLUSION

We demonstrate the emergence of superconductivity at the interface between the type-II Weyl semimetal WTe<sub>2</sub> and the normal metal palladium. Studying the transport properties in magnetic field and at different temperatures we deduce the key parameters that characterize the superconducting state, including the critical temperature  $T_c$ , the coherence length  $\xi$  and the London penetration depth  $\lambda_L$ . The combined set of parameters hint to a possible origin of superconductivity being due to the formation of flat bands. Moreover, the measured in-plane critical field exceeds the Pauli limit, suggesting non-trivial superconducting pairing. The coexistence of superconductivity with topological states makes WTe<sub>2</sub> a promising platform for topological superconductivity and applications for quantum computing.

## ACKNOWLEDGMENTS

We thank A. Baumgartner for helpful discussions. A.K. was supported by the Georg H. Endress foundation. This project has received further funding from the European Research Council (ERC) under the European Unions Horizon 2020 research and innovation programme: grant agreement No 787414 TopSupra, by the Swiss National Science Foundation through the National Centre of Competence in Research Quantum Science and Technology (QSIT), and by the Swiss Nanoscience Institute (SNI). K.W. and T.T. acknowledge support from the Elemental Strategy Initiative conducted by MEXT, Japan and the CREST (JPMJCR15F3), JST. D.G.M. and J.Y. acknowledge support from the U.S. Department of Energy (U.S.-DOE), Office of Science - Basic Energy Sciences (BES), Materials Sciences and Engineering Division. D.G.M. acknowledges support from the Gordon and Betty Moore Foundations EPiQS Initiative, Grant GBMF9069.

## DATA AVAILABILITY

All data in this publication are available in numerical form in the Zenodo repository at <https://doi.org/10.5281/zenodo.3934680>.

---

\* [Artem.Kononov@unibas.ch](mailto:Artem.Kononov@unibas.ch)

† [Christian.Schoenberger@unibas.ch](mailto:Christian.Schoenberger@unibas.ch)

- [1] Nayak, S., Simon, S.H., Stern, A., Freedman, M. & Sarma, S.D. Non-Abelian anyons and topological quantum computation. *Rev. Mod. Phys.* **80**, 1083 (2008).
- [2] Cho G.Y., Bardarson J.H., Lu Y.M. et al. Superconductivity of doped Weyl semimetals: finite-momentum pairing and electronic analog of the 3He-A phase. *Phys. Rev. B* **86**, 214514 (2012).
- [3] Wei H.Z., Chao S.P. and Aji V. Odd-parity superconductivity in Weyl semimetals. *Phys. Rev. B* **89**, 014506 (2014).
- [4] Bednik G., Zyuzin A.A., and Burkov A.A. Superconductivity in Weyl metals. *Phys. Rev. B* **92**, 035153 (2015).
- [5] Hosur P., Dai X., Fang. Z. et al. Time-reversal-invariant topological superconductivity in doped Weyl semimetals. *Phys. Rev. B* **90**, 045130 (2014).
- [6] Chan C. and Liu X.J. Non-Abelian Majorana modes protected by an emergent second Chern number. *Phys. Rev. Lett.* **118**, 207002 (2017).
- [7] Tang E. and Fu L. Strain-induced partially flat band, helical snake states and interface superconductivity in topological crystalline insulators. *Nat. Phys.* **10**, 964 (2014).
- [8] Soluyanov, A. A. et al. Type-II Weyl semimetals. *Nature* **527**, 495498 (2015).
- [9] Li, P. et al. Evidence for topological type-II Weyl semimetal WTe<sub>2</sub>. *Nat. Commun.* **8**, 2150 (2017).

- [10] Wang, Z., Wieder, B.J., Li, J., Yan, B. & Bernevig, B.A. Higher-Order Topology, Monopole Nodal Lines, and the Origin of Large Fermi Arcs in Transition Metal Dichalcogenides  $XTe_2$  ( $X=Mo,W$ ). *Phys. Rev. Lett.* **123**, 186401 (2019).
- [11] A. Kononov, G. Abulizi, K. Qu, J. Yan, D. Mandrus, K. Watanabe, T. Taniguchi, and C. Schnenberger, *Nano Lett.* **20**, 4228 (2020).
- [12] Choi, Y.-B. et al. Evidence of Higher Order Topology in Multilayer  $WTe_2$  from Josephson Coupling through Anisotropic Hinge States. *Nat. Mater.* (2020).
- [13] Huang, C. et al. Edge superconductivity in Multilayer  $WTe_2$  Josephson junction. *Natl. Sci. Rev.* nwaal14 (2020).
- [14] Fei, Z. et al. Edge conduction in monolayer  $WTe_2$ . *Nat. Phys.* **13**, 677 (2017).
- [15] Wu, S. Observation of the quantum spin Hall effect up to 100 Kelvin in a monolayer crystal. *Science* **359**, 76 (2018).
- [16] Kang, D. et al. Superconductivity emerging from a suppressed large magnetoresistant state in tungsten ditelluride. *Nat. Commun.* **6**, 7804 (2015).
- [17] Pan, X.-C. et al. Pressure-driven dome-shaped superconductivity and electronic structural evolution in tungsten ditelluride. *Nat. Commun.* **6**, 7805 (2015).
- [18] Asaba, T. et al. Magnetic Field Enhanced Superconductivity in Epitaxial Thin Film  $WTe_2$ . *Sci. Rep.* **8**, 6520 (2018).
- [19] Sajadi, E. et al. Gate-induced superconductivity in a monolayer topological insulator. *Science* **362**, 922 (2018).
- [20] Fatemi, V. et al. Electrically tunable low-density superconductivity in a monolayer topological insulator. *Science* **362**, p. 926 (2018).
- [21] Zhao, Y.F. et al. Anisotropic magnetotransport and exotic longitudinal linear magnetoresistance in  $WTe_2$  crystals. *Phys. Rev. B* **92**, 206803(R) (2015).
- [22] Blake, P. et al. Making graphene visible. *Appl. Phys. Lett.* **91**, 063124 (2007).
- [23] Zomer, P. J., Guimaraes, M. H. D., Brant, J. C., Tombros, N. & van Wees, B. J. Fast pick up technique for high quality heterostructures of bilayer graphene and hexagonal boron nitride. *Appl. Phys. Lett.* **105**, 013101 (2014).
- [24] Ali, M.N. et al. Correlation of crystal quality and extreme magnetoresistance of  $WTe_2$ . *EPL* **110**, 67002 (2015).
- [25] Xiang, F.X. et al. Thickness-dependent electronic structure in  $WTe_2$  thin films. *Phys. Rev. B* **98**, 035115 (2018).
- [26] Cao Y., Fatemi V., Demir A. et al. Correlated insulator behaviour at half-filling in magic-angle graphene superlattices. *Nature (London)* **556**, 80 (2018).
- [27] Tinkham, M. Introduction to superconductivity second edition. (McGraw-Hill, Inc., New York, 1996).
- [28] Y. Saito, T. Nojima, Y. Iwasa. Highly crystalline 2D superconductors. *Nat. Rev. Mater.* **2**, 16094 (2016).
- [29] R.A. Klemm, A. Luther, M.R. Beasley. Theory of the upper critical field in layered superconductors. *Phys. Rev. B* **12**, 877 (1975).
- [30] A.I. Gubin, K.S. Ilin, S.A. Vitusevich, M. Siegel, and N. Klein. Dependence of magnetic penetration depth on the thickness of superconducting Nb thin films. *Phys. Rev. B* **72**, 064503 (2005).
- [31] Shvetsov, O.O., Kononov, A., Timonina, A.V., Kolesnikov, N.N. & Deviatov, E.V. Realization of a Double-Slit SQUID Geometry by Fermi Arc Surface States in a  $WTe_2$  Weyl Semimetal. *JETP Lett.* **107**, 774 (2018).
- [32] Kononov, A. et al. Signature of Fermi arc surface states in Andreev reflection at the  $WTe_2$  Weyl semimetal surface. *EPL* **122**, 27004 (2018).
- [33] Zhu, Z. et al. Quantum oscillations, thermoelectric coefficients, and the Fermi surface of semimetallic  $WTe_2$ . *Phys. Rev. Lett.* **114**, 176601 (2015).
- [34] Yang, W. et al. The soft-mode phonons mediated unconventional superconductivity in monolayer  $1T'-WTe_2$ . Preprint at <https://arxiv.org/abs/2005.11012> (2020).
- [35] Shvetsov, O.O., Esin, V.D., Timonina, A.V., Kolesnikov, N.N. & Deviatov, E.V. Surface superconductivity in three-dimensional  $Cd_3As_2$  semimetal at the interface with a gold contact. *Phys. Rev. B* **99**, 125305 (2019).
- [36] Zhu W., Hou X., Li J. et al. Interfacial Superconductivity on the Topological Semimetal Tungsten Carbide Induced by Metal Deposition. *Adv. Mater.* **32**, 1907970 (2020).
- [37] Xing Y., Shao Z., Ge J. et al. Surface superconductivity in the type II Weyl semimetal  $TaIrTe_4$ . *Nat. Sc. Rev.* **7**, 579, (2020).
- [38] Shao, B. et al. Pseudodoping of a metallic two-dimensional material by the supporting substrate. *Nat. Commun.* **10**, 180 (2019).
- [39] Alidoust M., Halterman K., and Zyuzin A.A. Superconductivity in type-II Weyl semimetals. *Phys. Rev. B* **95**, 155124 (2017).
- [40] D.I. Indolese, R. Delagrance, P. Makk, J.R. Wallbank, K. Watanabe, T. Taniguchi, and C. Schnenberger. Signatures of van Hove singularities probed by the supercurrent in a graphene hBN superlattice. *Phys. Rev. Lett.* **121**, 137701 (2018).
- [41] V.J. Kauppila, F. Aikebaier, and T.T. Heikkil. Flat-band superconductivity in strained Dirac materials. *Phys. Rev. B* **93**, 214505 (2016).
- [42] Barash Yu.S. and Nagornykh P.I. Dispersionless modes and the superconductivity of ultrathin films. *JETP Lett.* **83**, 376 (2006).
- [43] Kopnin N.B., Heikkil T.T., and Volovik G.E. High-temperature surface superconductivity in topological flat-band systems. *Phys. Rev. B* **83**, 220503(R) (2011).